Defect Mediated Magnetic Interaction and High T_c Ferromagnetism in Co Doped ZnO Nanoparticles

Bappaditya Pal and P. K. Giri*

Department of Physics and Centre for Nanotechnology, Indian Institute of Technology, Guwahati 781039, India

Structural, optical and magnetic studies have been carried out for the Co-doped ZnO nanoparticles (NPs). ZnO NPs are doped with 3% and 5% Co using ball milling and ferromagnetism (FM) is studied at room temperature and above. A high Curie temperature (T_c) has been observed from the Co doped ZnO NPs. X-ray diffraction and high resolution transmission electron microscopy analysis confirm the absence of metallic Co clusters or any other phase different from würtzite-type ZnO. UV-visible absorption and photoluminescence studies on the doped samples show change in band structure and oxygen vacancy defects, respectively. Micro-Raman studies of doped samples shows defect related additional strong bands at 547 and 574 cm^{-1} confirming the presence of oxygen vacancy defects in ZnO lattice. The field dependence of magnetization (M–H curve) measured at room temperature exhibits the clear M–H loop with saturation magnetization and coercive field of the order of 4–6 emu/g and 260 G, respectively. Temperature dependence of magnetization measurement shows sharp ferromagnetic to paramagnetic transition with a high $T_C = 791$ K for 3% Co doped ZnO NPs. Ferromagnetic ordering is interpreted in terms of overlapping of polarons mediated through oxygen vacancy defects based on the bound magnetic polaron (BMP) model. We show that the observed FM data fits well with the BMP model involving localised carriers and magnetic cations.

Keywords: ZnO, Dilute Magnetic Semiconductors, Bound Magnetic Polaron, Co Doping.

RESEARCH ARTICLE

1. INTRODUCTION

Diluted magnetic semiconductors (DMS), where transition metal atoms are introduced into the cationic sites of the semiconducting host lattice, have recently attracted increasing attention because of their potential use in spintronic devices.[1–5] The main challenge in the practical applications of the DMS materials is the attainment of ferromagnetism (FM) above room temperature (RT) to be compatible with junction temperatures. Dietl et al.[3] predicted the existence of high-temperature FM in some magnetically doped wide band gap semiconductors. Among wide band gap semiconductors, ZnO has been considered as one of the promising candidates for fabricating DMS due to its high solubility for transition metals (TM) and superior semiconductor properties. Moreover, ZnO is a wide band gap (3.27 eV) semiconductor with a large exciton binding energy (60 mev) and has potential applications in electronic and optoelectronic devices.[6] Particularly, transition-metal-doped ZnO DMSs have been extensively investigated since theoretical studies

predicted it's Curie temperature (T_c) to be above room temperature. Recently, origin of FM ordering in pristine mirco- and nanostructured ZnO has been discussed and role of surface defect was emphasized.[7] However, the magnitude of FM in such undoped systems is usually too low for any practical application.

Despite large number of studies reported on ZnO-based DMSs, there is no clear agreement about the nature and origin of the magnetic properties of samples prepared by different methods and different groups.[8] Some reports suggested segregation and the formation of Co clusters as the origin of FM signal,[9] but more recent results seems to indicate the existence of intrinsic FM.[10–12] Ueda and Kawai reported FM with a Curie temperature higher than RT for the Co-doped ZnO films grown by the pulsed-laser deposition technique.[13] RT and high temperature FM has been reported on Co doped ZnO thin films by several groups.[14–16] Rao and Deepak observed the absence of ferromagnetism in Co-doped ZnO powder fabricated by the low-temperature decomposition of acetate solid solution.[17] These controversial results between research groups suggest that the magnetic properties of DMS materials seem to

---

*Author to whom correspondence should be addressed.

be very sensitive to the preparation method and the structure of materials.[7] Here we have doped Co in ZnO NPs by using a mechanical ball milling process and it proves to be an effective and simple technique to prepare TM doped semiconductors that exhibit high temperature FM.

In this work, we report on the magnetic, structural and optical properties of Co-doped ZnO NPs. X-ray diffraction (XRD) and transmission electron microscopy (TEM) are used to examine phase segregation and morphological analysis. Micro Raman and photoluminescence (PL) studies are performed to confirm the presence of defects in doped ZnO. UV-VIS optical absorption is used to infer the substitution of cobalt inside the Zn lattice corresponding to the bandgap shift. Vibrating sample magnetometer (VSM) is employed to measure the RT magnetic properties and the variation of magnetization with temperature. The observed magnetization and its temperature dependence are discussed with reference to the role of defects and doping concentration in the ZnO sublattice.

2. EXPERIMENTAL DETAILS

The starting materials are commercial ZnO nanopowder (purity 99.999%, Sigma Aldrich) and cobalt (Co) powder (99.5%, Loba Chemie). 3% and 5% Co powders are mixed with the ZnO nanopowder. After mixing, the powders are ground for 10 minutes and milled in a mechanical ball-milling machine (Retsch, PM 100) at 350 rpm for duration of 5 hrs and 8 hrs in a zirconium oxide vial under atmospheric pressure and temperature. Zirconium oxide balls of diameter 5 mm are used in this experiment. The ball to powder mixture weight ratio is taken as 10:1. Post-growth annealing is done for the 5 hrs milled sample at two different temperatures: 250 °C and 500 °C for 1 hrs.

The crystal structures of the obtained samples are characterized by XRD patterns (Bruker D8 Advance, CuK$_\alpha$ radiation) and micro-Raman spectroscopy (LabRam HR800, Jobin Yvon). Morphology and structures of as-synthesized samples are observed by high-resolution TEM (HRTEM) (JEOL-JEM 2010 operated at 200 keV). Specimens for HRTEM investigations are prepared by dispersing powder particles in methanol and drop casting it on a carbon coated copper grid of 400 mesh (Pacific Grid, USA). HRTEM imaging and microanalysis by energy-dispersive X-ray spectroscopy (EDS) are conducted in the same microscope. The magnetic properties of the samples are measured by using a Lakeshore (model no. 7410) VSM. The UV-Vis absorption spectroscopy measurements are recorded using a commercial spectrophotometer (Varian) with a monochromated Xenon lamp source. PL measurement was performed at RT using a 325 nm laser excitation coupled in a commercial high resolution fluorimeter (Edinburg, FSP920).

3. RESULTS AND DISCUSSION

3.1. Structural Characterization

Figure 1 shows some typical XRD patterns of the Co doped ZnO NPs. Figures 1(a–c) are for undoped, 3% doped and 5% doped NPs, respectively. For each sample, all the observed diffraction peaks can be indexed to a ZnO wurtzite structure (space group P6$_3$mc), and no other impurity phase was found, which indicates that the Co ions successfully occupy the lattice site rather than interstitial ones. In addition, very slow scans near the peaks of both hexagonal and cubic cobalt phases reveal no signatures of any kind of additional phases in the NPs. XRD Measurement of Co powder shows one intense peak around 44° which does not appear for the doped samples indicating Co is doped well in the ZnO sublattice. Compared to undoped ZnO, the doped samples shows lowering of intensity and increase in full width at half maxima (FWHM) of the XRD pattern. NP size is reduced considerably for the doped samples during milling compared to undoped NPs as shown in Table I. Interestingly, a slow scan comparison of the (101) peak of Co-doped and the undoped ZnO NPs show a higher 2θ value and lower intensity for the doped ZnO NPs, as shown in the inset of Figure 1. The change in the XRD pattern in doped samples is attributed to size reduction and lattice strain induced by the ball milling. Since the ionic radius of Co and Zn are very close, Co doping induced strain is expected to be less significant. However, as a result of ball milling, a compressive strain is introduced in the ZnO NPs.[18] From the measured shift in 2θ for (101) plane, we estimate a reduction in interplanar spacing (d_{101}) of ~0.38%. This strain in the NPs
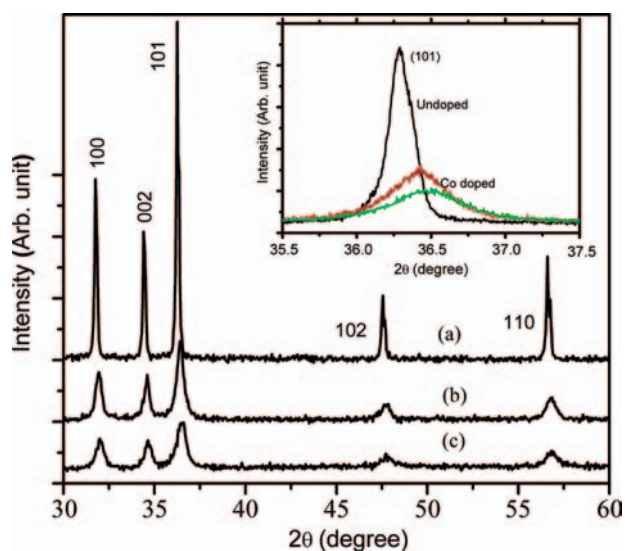
Fig. 1. XRD pattern of the Co-doped ZnO NPs: (a) undoped (b) 3% Co doped (c) 5% Co doped; The inset shows high resolution XRD data of the (101) peak for undoped and doped ZnO NPs. Peak shift is evident in Co doped NPs.

Table I. 3% and 5% Co doped ZnO NPs: Crystallite size determined from XRD profile; saturation magnetization (M_s), coercive filed (H_c) and remanent magnetization (M_r) are determined from M–H curves; transition temperature (T_c) is determined from differentiated M–T curves. M_0, m_{eff}, χ_m, N are determined from fitting of the M–H curve with BMP model (Eq. (1)).

Co doping concentration	Crystallite size (nm)		M_s (emu/g)	H_c (Gauss)	M_r (emu/g)	T_c (K)	Fitting parameters extracted from BMP model			
	Undoped	Doped					M_0 (emu/g)	m_{eff} (emu) $\times 10^{-17}$	$\chi_m \times 10^{-5}$	$N \times 10^{17}$ (cm^{-3})
3%	81.8	21.7	3.95	268	0.42	791	4.47	3.43	1.24	7.32
5%	81.8	18.1	5.91	263	0.68	—	6.40	4.03	0.64	8.90
3%, 250 °C annealed	81.8	—	4.21	250	0.35	—	—	—	—	—
5%, post M–T	42.4	—	0.59	204	0.09	—	—	—	—	—

is expected to influence the electronic properties including band-structure of ZnCoO.

Figure 2(a) shows low-magnification scanning electron microscopy (SEM) images of the undoped ZnO NPs and Figure 2(b) shows TEM image of the 3% Co doped ZnO NPs prepared after 5 hrs of milling. The micrograph reveals NP size distribution in the range 80–100 nm for undoped NPs, similar to the size estimated from XRD profile line width. For the doped ZnO, the average size of the NPs is about 20–25 nm. Different kinds of shapes of the NPs are discernible in Figure 2(a): irregularly shaped particle, larger rectangular platelets and hexagonally shaped particles. However, doped NPs are of regular shapes, mostly spherical. HRTEM lattice images are presented in Figure 2(c), which shows that all the NPs are single crystalline and devoid from any major lattice defects. The d-spacing of the crystal plane is calculated as 0.244 nm which shows the preferable crystal growth plane is (101) and it is also the highest intensity peak in the XRD pattern shown in Figure 1. The crystallinity and preferential orientation of the NPs in the sample are confirmed
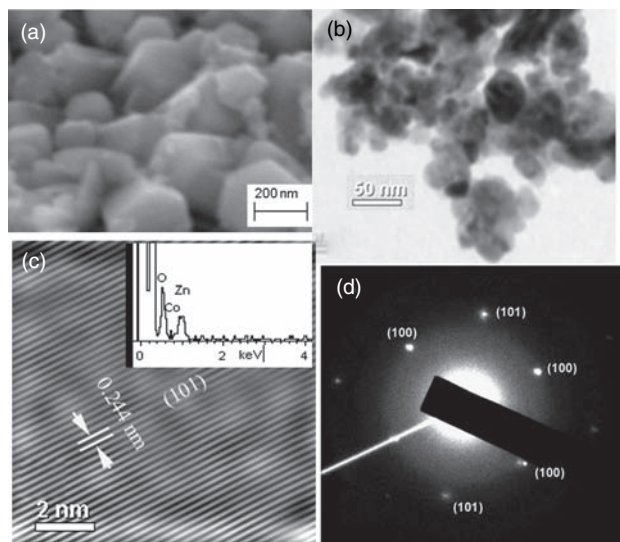
from the selected area diffraction (SAD) patterns shown in Figure 2(d), confirming that the ZnCoO NPs are single crystals. The SAD pattern obtained by focusing the beam on a few NPs of the sample clearly indicates the single crystalline nature of each NPs. Also, it confirms that the nanocrystals are indeed in the wurtzite phase. Due to low doping concentration, there is no cobalt clusters observed in the as-prepared NPs. In the EDS spectrum measured on few single particle of the as-prepared ZnCoO, Zn, Co, and O related peaks are seen as shown in inset of Figure 2(d), besides Cu and C peaks from carbon coated Cu grid used in TEM. This indicates that cobalt ions were uniformly distributed in the entire ZnCoO samples.

3.2. Raman Scattering Studies

In order to investigate the influence of Co doping on microstructure and vibrational properties, Raman scattering experiments were carried out. Raman scattering is a versatile technique for detecting the incorporation of dopants and the resulted defects and lattice disorder in the host lattice.[19] The zone-centre optical phonons of the wurtzite structure of ZnO can be classified according to the following irreducible representations: $\Gamma_{opt} = A_1 + E_1 + 2E_2 + 2B_1$. The B_1 modes are silent in Raman scattering, whereas A_1 and E_1 modes are polar and hence exhibit different frequencies for the transverse-optical (TO) and longitudinal-optical (LO) phonons.[20] The non-polar E_2 modes have two frequencies, namely, E_2 (high) and E_2 (low) associated with the motion of oxygen (O) atoms and zinc (Zn) sublattice, respectively.[21] Figure 3 shows the room-temperature Raman spectrum of undoped and doped samples in the range 200 to 800 cm^{-1}. For the undoped ZnO, the sharpest and strongest peak at ∼437 cm^{-1} can be assigned to E_2 (high), which is the strongest mode in wurtzite crystal structure. The peaks at 330 and 379 cm^{-1} are assigned to the second-order vibration mode and A1(TO) mode, respectively. In the doped NPs, the broad peak is deconvoluted into two peaks, as shown in inset of Figure 3. The peak at 574 cm^{-1} is the E1(LO) mode and can be attributed to defects due to O vacancies, Zn interstitial defect states.[22] Compared with the undoped ZnO NPs, additional strong peaks can

Fig. 2. (a) SEM image of the morphology of the undoped ZnO NPs, (b) TEM image of the doped (3% Co) NPs, (c) HRTEM lattice image of doped NPs showing no clustering of Co, inset shows EDS spectrum showing presence of Co in ZnO NPs, (d) corresponding SAED pattern.
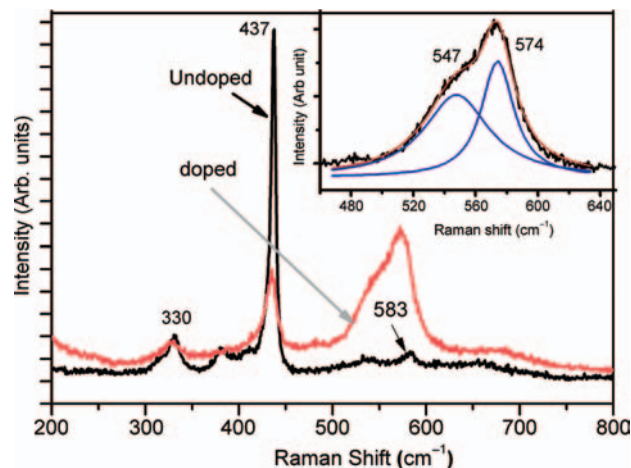
Fig. 3. Raman spectra for the undoped and 3% Co doped ZnO NPs: The inset on the upper right corner shows the magnified view of the defect related Raman bands in the in Co-doped NPs. Two peaks are fitted with Lorentzian line shape.

be observed at ~547 and ~574 cm^{-1} in the Raman spectrum of the $Zn_{1-x}Co_xO$ ($x = 0.03, 0.05$). Wang et al.[19] and Cheng et al.[23] also observed this mode in (Co, Al) and Ce-doped ZnO. According to the literature, this mode is induced by host lattice defects, such as oxygen vacancies and Zn interstitials. With the doping content, the host lattice defects in ZnO are activated and amplified and then this mode appears. In the present case, due to the smaller ionic radius of Co^{2+} than that of Zn^{2+}, when Co^{2+} was doped into ZnO lattice, more oxygen vacancies and Zn interstitials are created. Therefore, the appearance of 547 and 574 cm^{-1} can be used to characterize Co^{2+} doped into ZnO lattice.[24]

3.3. Optical Absorption and Photoluminescence Studies

Many groups have confirmed that Co atomically substitutes on Zn sites using a variety of optical methods such as X-ray photoelectron spectroscopy[26] and optical absorption.[25–26] The four-fold coordinated ionic radii of Co^{+2} (0.058 nm) and Zn^{+2} (0.06 nm) are very similar and results in a large solubility of Co^{+2} in the ZnO lattice.[27] Evidence for Co substitution in the ZnO lattice can be inferred from optical UV-VIS absorption spectrum. The UV-VIS absorption spectrum was used primarily to find possible change in the band gap. Figure 4(a) shows the UV-VIS spectrum taken at room temperature. The change in absorption peak due to doping indicates a change in the band structure. A blue-shift is observed in the bandgap energy for the cobalt doped samples compared to the undoped ZnO. Since the NP sizes are larger than excitonic Bohr radius in ZnO, size effect is unlikely to cause the observed blue shift. It is the strain that causes the change in the bandstrcture of doped ZnO. The *sp–d* exchange between the ZnO band electrons and localized *d*-electrons
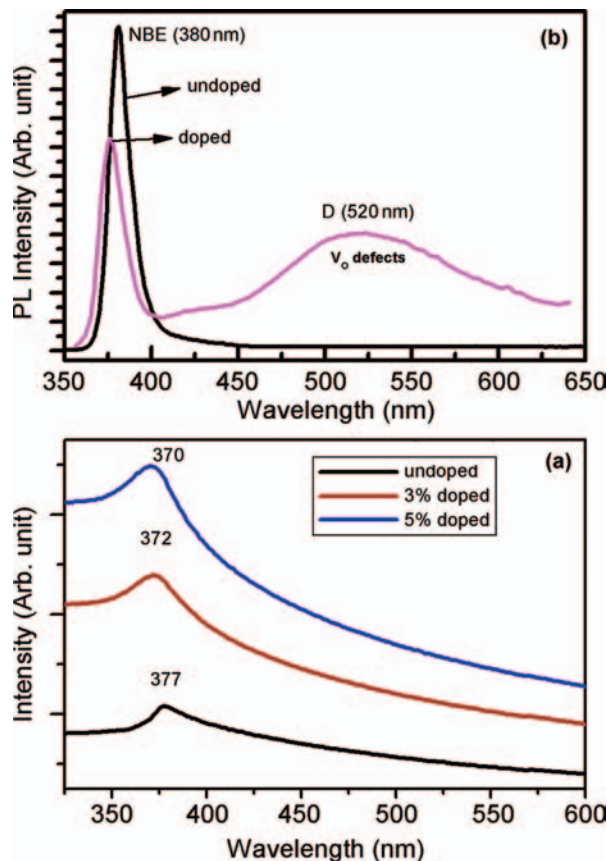
Fig. 4. (a) UV-Vis absorption spectrum of undoped and Co doped ZnO NPs (3% and 5%) showing clear blue shift for doped NPs. (b) PL spectra of undoped and doped ZnO NPs. Defect related visible emission band (D-band) is shown to be strong in doped ZnO NPs.

associated with the doped Co^{+2} cations may cause the change in such band-structure. The interaction leads to corrections in the energy bands.[28]

The PL spectra of the undoped and Co-doped ZnO NPs recorded at RT are shown in Figure 4(b). There are two distinct emission bands in the spectra of the NPs, one peak is in the UV region (~380 nm) and another broad visible emission at 520 nm due to the intrinsic defect related band (D). As compared to the undoped NP, the UV emission peak for the doped NP is found to be blue shifted and intensity reduced. The ~380 nm peak usually originates from the near band-edge (NBE) transition of ZnO and is generally attributed to the recombination of free excitons.[29] The blue-shift indicates a higher band gap for the doped NP that may be caused by strain[18] since the NP sizes are much above the excitonic Bohr diameter of ZnO. The D band is centred at ~520 nm and it is observed that the D band becomes very intense with doping of Co in ZnO NPs. It is often attributed to the radiative recombination of photogenerated holes with electrons occupying the singly ionized oxygen vacancy (V_o).[30, 31] Based on the band-structure calculations the visible emission has been assigned to V_o and Zn_{in}.[32] Therefore, it is believed that the

observed strong visible emission in doped ZnO originates from the deep levels of Co-doped ZnO NPs and is due to the presence of V_o and Zn_{in} defects. Thus, PL studies confirm the presence of oxygen vacancy defects in doped ZnO NPs and this is consistent with the Raman analysis.

3.4. Magnetic Characterization

The magnetic properties of the Co-doped ZnO NPs were investigated using VSM. We observed distinct ferromagnetic behaviour at room temperature in the doped samples only. Despite the presence of some intrinsic defects in undoped ZnO NPs, no trace of FM was observed in the undoped sample that was first tested under similar conditions using the VSM. Figure 5 shows the magnetic hysteresis (*M–H*) loops for 3% and 5% doped NPs measured at 300 K. The inset shows a magnified view of the *M–H* loop showing distinct hysteresis effect. The saturation magnetizations (M_s) of the samples vary in the range of 3.95–5.91 emu/g with a coercive filed (H_c) of ~260 G for the 5 hrs milled sample. The changes of M_s and H_c for different doping concentrations are compared as shown in Table I. Post growth annealing in air atmosphere at 250°C affects the magnetization. M_s first increases for 250 °C annealing and then it decreases to a low value for annealing at 500 °C due to paramagnetic transition process (see Table I). Same kind of variation in magnetization can be
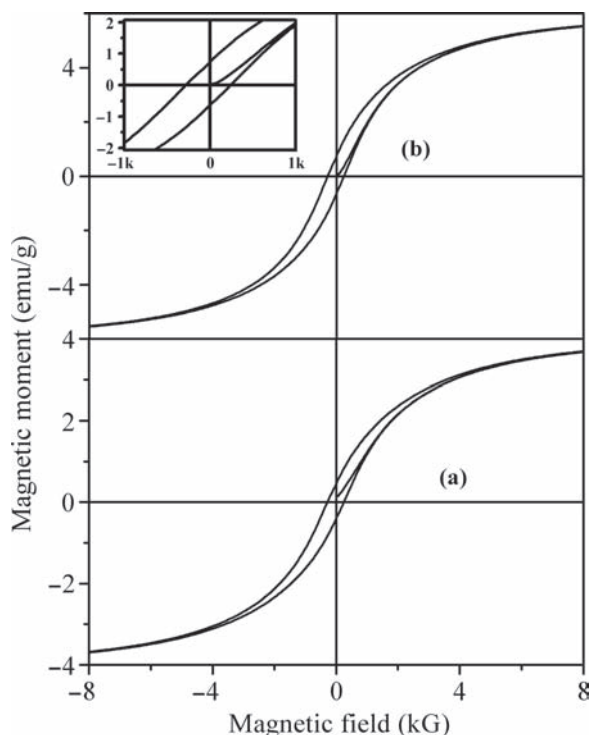
seen in the magnetization versus temperature (*M–T*) data shown below where magnetization increases slowly before starting transition towards paramagnetic nature.

It is well known that for use in a wide range of applications without temperature control, the ferromagnet should have a T_C enough above RT (300 K). Figure 6 shows the temperature dependent magnetization of doped NPs in the range 300 To 900 K. From the differential plot of the *M–T* curve we obtained a $T_c = 791$ K, which implies that the ferromagnetism is not due to the Co metal ($T_c > 1300$ K). As seen from the *M–T* curve, at higher temperature (>700 K) the magnetization shows a rapid decrease with temperature. The magnetization measurement at 300 K of the post *M–T* measurement, i.e., the Co: ZnO NPs annealed at 850 K in ambient condition shows that the magnetic moment is significantly reduced, which decreases to 0.59 emu/g for the 5% Co doped sample. This magnetic transition suggests that high-temperature process causes a rapid destruction of ferromagnetic coupling. Note that compared to the 3% doped samples, 5% doped samples did not exhibit proper sharp transition at higher temperature. The absence of a sharp FM to paramagnetic transition in *M–T* curve for higher doped (5% Co) ZnO NPs may be because of possible antiferromagnetic interaction due to the reduction in average interatomic distance of doped Co ions. Thus, 3% doping of small size NPs is found to yield best result for the observed high temperature FM.

3.5. Origin of the FM

The origin of observed FM at room temperature in these NPs could arise from a number of sources, such as the intrinsic property of the doped NPs, formation of some nanoscale Co-related secondary phase, Co precipitation and CoO. However, CoO phase can be easily ruled out, since CoO is antiferromagnetic with a Neel temperature of

Fig. 5. Room temperature field versus magnetization (*M–H*) loop showing hysteresis of the Co doped ZnO NPs: (a) 3% Co doped, (b) 5% Co-doped. The inset shows the magnified *M–H* loop showing clear ferromagnetic hysteresis behaviour. Measured parameters are listed in Table I.
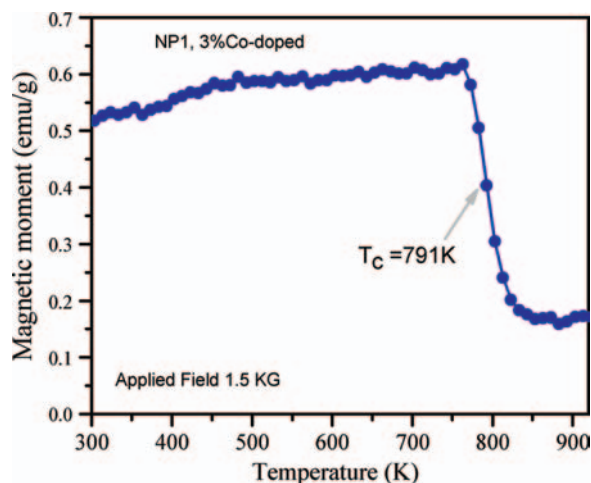
Fig. 6. Temperature dependent magnetization (*M–T*) curve of 3% Co doped ZnO NP showing high transition temperature (T_c) and sharp ferromagnetic to paramagnetic transition.

293 K. Secondly, metallic Co is also an unlikely source of this ferromagnetism, as XRD and HRTEM results show no metallic Co clusters in the NPs. UV-VIS absorption, showed a band-gap modification which suggests Co^{2+} ions were successfully incorporated into the wurtzite lattice at the Zn^{2+} sites. Therefore FM is expected to arise from the intrinsic exchange interaction of magnetic moments in doped NPs.

There are several mechanisms proposed in the literature regarding the origin of ferromagnetism in DMSs. The exact mechanism of intrinsic ferromagnetism in TM-doped oxides is still under debate. A diversity of theories has been proposed, such as Ruderman-Kittel-Kasuya-Yosida (RKKY) interaction, super-exchange, double-exchange between the d states of TMs, free-carrier-mediated exchange and sp–d exchange mechanism, etc.[33] The RKKY interaction is based on free electrons, but ZnO cannot transform into a metal at such a low doping. Direct interactions such as double-exchange or super-exchange cannot be responsible for the ferromagnetism because the magnetic cations are dilute in our samples. All these proposed theories cannot well accord with the experimental results in DMSs.[34] According to the literature, magnetic cations, carriers and defects can make up bound magnetic polarons (BMPs). In addition to the magnetic doping effect, oxygen vacancy (V_o) defects have been suggested to play an important role in the magnetic origin for oxide DMSs.[35] Interestingly, very recent report shows that TM site in Co-doped ZnO does not yield any FM.[36] The authors concluded that magnetic properties could arise from delocalized magnetic moments, due to itinerant electrons associated with defects, such as oxygen vacancies and interstitial dopant ions. Theoretical studies suggest that V_o can cause an obvious change of the band structure of host oxides and makes a significant contribution to the ferromagnetism.[37, 38] The formation of BMPs, which include electrons locally trapped by oxygen vacancy, with the trapped electron occupying an orbital overlapping with the d shells of TM neighbors, has also been proposed to explain the origin of FM.[37] Oxygen vacancies are present large concentration in as grown ZnO NPs due to the stabilization of structure. On the basis of observed intense defect modes seen in Raman and PL spectra, we presume that oxygen vacancies play a key role in the observed FM at room temperature and above. We notice that post growth air annealing at 250 °C shows increase of M_s owing to the increase of O-vacancy or vacancy clusters that helps to create more BMPs and their percolation.[39] Our systematic study shows that oxygen-vacancy defect constituted BMPs are most promising candidate for the origin of room-temperature FM in this system. Within the BMP model, the greater density of oxygen vacancy (V_o) and more doping help to produce more BMPs which yields a greater overall volume occupied by BMPs, leading to the overlap of BMPs and enhancing FM. This evolution is observed

in our case, increase of magnetization with the Co concentration indicating that the FM in our samples is due to percolation of BMPs.

To understand further about the more specific nature of magnetic interaction, we have fitted the M versus H data to the BMP model by following Chiorescu et al.[40] According to the BMP model, the measured magnetization can be fitted to the relation:

$$M = M_0 L(x) + \chi_m H \qquad (1)$$

where the first term is from BMP contribution and the second term is due to paramagnetic matrix contribution. Here $M_0 = Nm_s$, N is the number of BMPs involved and m_s is the effective spontaneous moment per BMP. $L(x) = \coth(x) - 1/x$ is the Langevin function with $x = m_{eff}H/(k_B T)$, where m_{eff} is the true spontaneous moment per BMP, and at higher temperature it can be approximated to $m_s = m_{eff}$. We have analyzed the M–H curve by using Eq. (1). The parameters M_0, m_{eff} and χ_m are variable in the fitting process. The experimental data along with fitted data are shown in Figure 7 for the 3% Co doped $Zn_{1-x}Co_xO$ sample at 300 K. It is evident that fitted data closely follows the experimental data implying the suitability of BMP model in the observed FM. The fitted parameters are tabulated in Table I. The total BMP magnetization M_0 values are found to be of the order of 4 emu/g. The M_0 value is found to increase with increase in doping concentration. The paramagnetic susceptibility χ_m is found to be of the order of 10^{-5} and its value marginally changes with doping. The spontaneous moment per BMP, m_{eff} is found to be in the order of 10^{-17} emu. By assuming $m_s = m_{eff}$, we have estimated the concentration of BMP, which was found to be in the order of 10^{18} cm^{-3}. Note that calculated concentration of the BMPs is about two orders
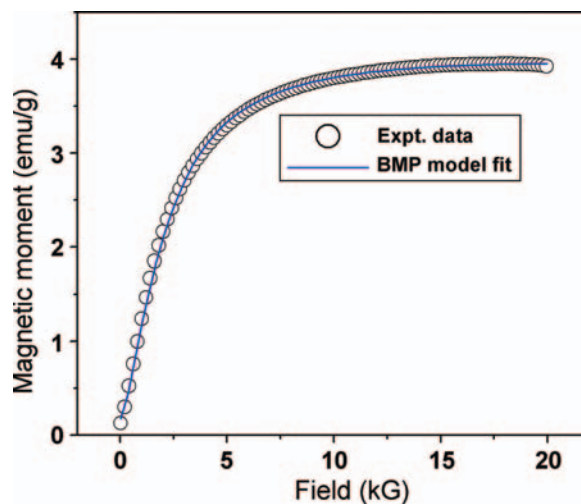
Fig. 7. Initial portion of the M–H curve fitted with BMP model (Eq. (1)) for 3% Co doped ZnO NPs. Symbols are for experimental data and the solid line is a fit with BMP model. Extracted parameters are shown in Table I.

of magnitude lower than the typical percolation threshold in ZnO.[37] Despite the relatively high concentration of Co ions (3–5%), the concentration of BMPs is limited by the availability of free carriers in the ZnCoO samples. Thus, our results could be explained based on the BMP model. Similar BMP model was invoked recently to explain the RT ferromagnetism in Ni doped ZnO.[41]

Note that very few studies have reported such high M_s value at room temperature in the Co-doped ZnO as observed in this study. A majority of the previous studies on Co doping have been carried out on bulk ZnO or thin film of ZnO. The FM in such systems has been reported to be dependent on process condition. It is likely that due to inadequate density of interacting defects, free carriers, magnetic impurity forming BMPs, a relatively weak FM is observed at or above RT. However, small NPs of ZnO may show enhanced magnetic properties that the bulk counter part. In the present case, due to small size of the NPs and presence of lattice strain, there is likely to have enhanced confinement effect on the magnetic interaction that leads to formation of large number of BMP even at room temperature. Our XRD results have shown substantial amount of strain the Co doped ZnO NPs due to the specific method of preparation. We believe that among the other factors, lattice strain in doped ZnO NPs plays a definite role in the observed high temperature FM. It may be noted that in our study 250 °C annealed samples where strain is expected to be reduced shows marginally higher M_s value. A controlled amount of strain may be helpful in engineering the FM ordering in these NPs. Further, low temperature annealing may cause formation of vacancy clusters that help in forming more BMPs and thus higher M_s is obtained. It is well known that for semiconductor NPs, strain modified the electronic band structure including increase in band gap. It has been reported that strained Si NPs shows enhanced confinement effect of carriers than unstrained NPs.[42] Thus, strain induced enhanced confinement may be partly responsible for the enhanced FM interaction in these doped ZnO NPs. This study shows that strain engineering of DMS materials may add new dimensionality to control and achieve the high temperature FM in such materials.

4. CONCLUSION

In conclusion, nanocrystalline ZnCoO has been synthesized by a simple ball milling method using ZnO NPs. Microstructure analysis shows that the NPs are of single crystalline ZnO wurtzite structure. XRD, HRTEM, EDS, UV-VIS absorption measurements indicate that Co^{2+} substitute into ZnO lattice at Zn^{2+} site. Raman scattering studies confirm the presence of large amount defects in the doped NPs. We argued that the observed FM in Co doped ZnO NPs is intrinsic and is due to percolation of BMPs; magnetic cations, carriers and defects make up BMPs. Our

data fits well to the BMP model and various parameter extracted from fitting are found to be in agreement with literature report. We believe that among the other factors, lattice strain in the doped NPs is believed to play a considerable role in the observed FM. In this work, RT FM have been obtained in Co doped ZnO DMSs material and it's Curie temperature (T_c) 791 K is much above room temperature. It is considered to be an important step for the development of semiconductor devices that can retain their FM properties above RT for the realization of practical commercial devices.

References and Notes

1. S. J. Pearton, C. R. Abernathy, D. P. Norton, A. F. Hebard, Y. D. Park, L. A. Boatner, and J. D. Budai, *Mater. Sci. Eng. R* 40, 137 (**2003**).
2. H. Ohno, *Science* 281, 951 (**1998**).
3. T. Dietl, H. Ohno, F. Matsukura, J. Cibert, and D. Ferrand, *Science* 287, 1019 (**2000**).
4. Y. Matsumoto, M. Murakami, T. Shono, T. Hasegawa, T. Fukumura, M. Kawasaki, P. Ahmet, T. Chikyow, S. Koshihara, and H. Koinuma, *Science* 291, 854 (**2001**).
5. P. Sharma, A. Gupta, K. V. Rao, F. J. Owens, R. Sharma, R. Ahuja, J. M. O. Guillen, B. Johansson, and G. A. Gehring, *Nat. Mater.* 2, 673 (**2003**).
6. S. J. Pearton, D. P. Norton, K. Ip, Y. W. Heo, and T. Steiner, *Superlatt. Microstruct.* 34, 3 (**2003**).
7. R. Podila, W. Queen, A. Nath, J. T. Arantes, A. L. Schoenhalz, A. Fazzio, G. M. Dalpian, J. He, S. J. Hwu, M. J. Skove, and A. M. Rao, *Nano Lett.* 10, 1383 (**2010**).
8. T. Fukumura, Y. Yamada, H. Toyosaki, T. Hasegawa, H. Koinuma, and M. Kawasaki, *Appl. Surf. Sci.* 223, 62 (**2004**).
9. S. A. Chambers, T. Droubay, C. M. Wang, A. S. Lea, R. F. C. Farrow, L. Folks, V. Deline, and S. Anders, *Appl. Phys. Lett.* 82, 1257 (**2003**).
10. Y. Zou, Z. Qua, J. Fang, and Y. Zhang, *J. Magn. Magn. Mater.* 321, 3352 (**2009**).
11. J. Iqbal, B. Wang, X. Liu, D. Yu, B. He, and R. Yu, *New J. Phys.* 11, 063009 (**2009**).
12. S. Ghoshal and P. S. Anil Kumar, *J. Magn. Magn. Mater.* 320, L93 (**2008**).
13. K. Ueda Tabata, H. Tabata, and T. Kawai, *Appl. Phys. Lett.* 79, 988 (**2001**).
14. C. Song, F. Zeng, K. W. Geng, X. B. Wang, Y. X. Shen, and F. Pan, *J. Magn. Magn. Mater.* 309, 25 (**2007**).
15. S. Deka, R. Paricha, and P. A. Joy, *Chem. Mater.* 16, 1168 (**2004**).
16. O. D. Jayakumar, I. K. Gopalakrishnan, C. Sudakar, R. M. Kadam, and S. K. Kulshreshtha, *J. Alloys Compnd.* 438, 258 (**2007**).
17. C. N. R. Rao and F. L. Deepak, *J. Mater. Chem.* 15, 573 (**2005**).
18. P. K. Giri, S. Bhattacharyya, D. K. Singh, R. Kesavamoorthy, B. K. Panigrahi, and K. G. M. Nair, *J. Appl. Phys.* 102, 093515 (**2007**).
19. J. B. Wang, G. J. Huang, X. L. Zhong, L. Z. Sun, Y. C. Zhou, and E. H. Liu, *Appl. Phys. Lett.* 88, 252502 (**2006**).
20. K. Samanta, P. Bhattacharya, R. S. Katiyar, W. Iwamoto, P. G. Pagliuso, and C. Rettori, *Phys. Rev. B* 73, 245213 (**2006**).
21. D. G. Mead and G. R. Wilkinson, *J. Raman Spectrosc.* 6, 123 (**1997**).

RESEARCH ARTICLE

22. J. Alaria, H. Bieber, S. Colis, G. Schmerber, and A. Dinia, *Appl. Phys. Lett.* 88, 112503 **(2006)**.

23. B. C. Cheng, Y. H. Xiao, G. S. Wu, and L. D. Zhang, *Appl. Phys. Lett.* 84, 416 **(2004)**.

24. L. B. Duan, G. H. Rao, Y. C. Wang, J. Yu, and T. Wang, *J. Appl. Phys.* 104, 013909 **(2008)**.

25. A. C. Tuan, J. D. Bryan, A. B. Pakhomov, V. Shutthanandan, S. Thevuthasan, D. E. McCready, D. Gaspar, M. H. Engelhard, J. W. Rogers, Jr., K. Krishnan, D. R. Gamelin, and S. A. Chambers, *Phys. Rev. B* 70, 054424 **(2004)**.

26. K. Samanta, P. Bhattacharya, and R. S. Katiyar, *Appl. Phys. Lett.* 87, 101903 **(2005)**.

27. Z. Jin, M. Murakami, T. Fukumura, Y. Matsumoto, A. Ohtomo, M. Kawasaki, and H. Koinuma, *J. Cryst. Growth* 214–215, 55 **(2000)**.

28. S. Guha, K. Ghosh, J. G. Keeth, S. B. Ogale, and S. R. Shinde, J. R. Simpson, H. D. Drew, and T. Venkatesan, *Appl. Phys. Lett.* 83, 16 **(2003)**.

29. C. Li, G. Fang, Q. Fu, F. Su, G. Li, X. Wu, and X. Zhao, *J. Cryst. Growth* 292, 19 **(2006)**.

30. H. T. Ng, B. Chen, J. Li, J. Han, M. Meyyappan, J. Wu, S. X. Li, and E. E. Haller, *Appl. Phys. Lett.* 82, 2023 **(2003)**.

31. C. W. Cheng, G. Y. Xu, H. Q. Zhang, and Y. Luo, *Mater. Lett.* 62, 1617 **(2008)**.

32. X. Liu, X. Wu, H. Cao, and R. P. H. Chang, *J. Appl. Phys.* 95, 3141 **(2004)**.

33. V. A. Fonoberov, K. A. Alim, A. A. Balandin, F. Xiu, and J. Liu, *Phys. Rev. B* 73, 165317 **(2006)**.

34. S. J. Pearton, W. H. Heo, M. Ivill, D. P. Norton, and T. Steiner, *Semicond. Sci. Technol.* 19, R59 **(2004)**.

35. H. S. Hsu, J. C. A. Huang, Y. H. Huang, Y. F. Liao, M. Z. Lin, C. H. Lee, J. F. Lee, S. F. Chen, L. Y. Lai, and C. P. Liu, *Appl. Phys. Lett.* 88, 242507 **(2006)**.

36. A. D. Trolio, R. Larciprete, S. Turchini, and N. Zema, *Appl. Phys. Lett.* 97, 052505 **(2010)**.

37. J. M. D. Coey, M. Venkatesan, and C. B. Fitzgerald, *Nat. Mater.* 4, 173 **(2005)**.

38. J. E. Jaffe, T. C. Droubay, and A. A. Chambers, *J. Appl. Phys.* 97, 73908 **(2005)**.

39. K. R. Kittilstved, N. S. Norberg, and D. R. Gamelin, *Phys. Rev. Lett.* 94, 147209 **(2005)**.

40. C. Chiorescu, J. L. Cohin, and J. J. Neumeier, *Phys. Rev. B* 76, 020404(R) **(2007)**.

41. B. Pandey, S. Ghosh, P. Srivastava, P. Kumar, D. Kanjilal, S. Zhou, and H. Schmidt, *J. Appl. Phys.* 107, 023901 **(2010)**.

42. A. Thean and J. P. Leburton, *Appl. Phys. Lett.* 79, 1030 **(2001)**.

RESEARCH ARTICLE